Saaki TNV, Strahl H, Hamoen LW.

Membrane curvature and the Tol-Pal complex determine polar localization of the chemoreceptor Tar in *E. coli*.

***Journal of Bacteriology* 2018**

DOI: https://doi.org/10.1128/JB.00658-17

Membrane curvature and the Tol-Pal complex determine polar localization of the chemoreceptor Tar in *E. coli*

Terrens N. V. Saaki [1], Henrik Strahl [2], Leendert W. Hamoen [1,#]

[1] Swammerdam Institute for Life Sciences, University of Amsterdam, Science Park 904, 1098 XH Amsterdam, The Netherlands

[2] Centre for Bacterial Cell Biology, Institute for Cell and Molecular Biosciences, Newcastle University, Newcastle NE2 4AX, United Kingdom

[#] For correspondence: L. W. Hamoen, Email: l.w.hamoen@uva.nl, Tel.: 0031-615085377

Running title: Membrane curvature and Tol-Pal drive Tar localization

Abstract

Chemoreceptors are localized at the cell poles of *Escherichia coli* and other rod-shaped bacteria. Over the years different mechanisms have been put forward to explain this polar localization; from stochastic clustering, membrane curvature driven localization, interactions with the Tol-Pal complex, to nucleoid exclusion. To evaluate these mechanisms, we monitored the cellular localization of the aspartate chemoreceptor Tar in different deletion mutants. We did not find any indication for either stochastic cluster formation or nucleoid exclusion. However, the presence of a functional Tol-Pal complex appeared to be essential to retain Tar at cell poles. Interestingly, Tar still accumulated at midcell in *tol* and in *pal* deletion mutants. In these mutants, the protein appears to gather at the base of division septa, a region characterised by strong membrane curvature. Chemoreceptors, like Tar, form trimer-of-dimers that bend the cell membrane due to a rigid tripod structure. The curvature approaches the curvature of the cell membrane generated during cell division, and localization of chemoreceptor tripods at curved membrane areas is therefore energetically favourable as it lowers membrane tension. Indeed, when we introduced mutations in Tar that abolish the rigid tripod structure, the protein was no longer able to accumulate at midcell or cell poles. These findings favour a model where chemoreceptor localization in *E. coli* is driven by strong membrane curvature and association with the Tol-Pal complex.

Importance

Bacteria have exquisite mechanisms to sense and to adapt to the environment they live in. One such mechanism involves the chemotaxis signal transduction pathway, in which chemoreceptors specifically bind certain attracting or repelling molecules and transduce the signals to the cell. In different rod-shaped bacteria, these chemoreceptors localize specifically to cell poles. Here, we examined the polar localization of the aspartate chemoreceptor Tar in *E. coli*, and found that membrane curvature at cell division sites and the Tol-Pal protein complex, localize Tar at cell division sites, the future cell poles. This

study shows how membrane curvature can guide localization of proteins in a cell.

Introduction

Bacteria use specific chemotaxis systems to sense chemical changes in their environment and respond accordingly. One of the best-known systems is that of *Escherichia coli*, which comprises five different membrane spanning chemoreceptors. The cytoplasmic domains of chemoreceptors associate with the adaptor protein CheW and with the histidine kinase CheA. The presence of repellents or absence of attractants results in increased CheA activity and subsequent increased levels of phosphorylated CheY, which acts on the flagellar motor to change rotation direction. Sensitivity of the chemoreceptors is tuned by methylation and demethylation for which the methylesterase CheB and methyltransferase CheR are responsible. The chemoreceptors are therefore also referred to as methyl-accepting chemotaxis proteins or MCPs. For an in-depth review on the chemotaxis system see e.g. (1, 2).

MCPs form large protein clusters together with CheW, -Y, -A, -B and –R at the cell poles of different bacteria including the Gram-negative model system *E. coli* and the Gram-positive model system *Bacillus subtilis* (3, 4). Several mechanisms have been proposed for this polar localization. In long filamentous *E. coli* cells, YFP labelled CheR clusters were found to assemble with a certain periodicity along the cell axis that corresponds to the position of future division sites. This model is referred to as the ‘stochastic nucleation model’ (5-7). Another theory postulated that MCPs preferably assemble at the curved membrane of cell poles (8). Chemoreceptors form membrane spanning trimers-of-dimers that interact at their cytoplasmic domain at a slight angle thereby forming a tripod-like configuration (9). Consequently, the trimer-of-dimers prefer bend membrane areas due to the reduced curvature mismatch (10, 11). This model was recently supported by mechanically bending of whole *E. coli* cells in curved micro-chambers (12), and was also shown to be the main mechanism by which the chemoreceptor TlpA of *B. subtilis* is localized (13). However, another study suggested that polar curvature is not crucial for the localization of chemoreceptor proteins in *E. coli*, but that this requires interaction with the Tol-Pal complex

(14). The trans-envelope Tol-Pal complex is a widely conserved component of the cell envelope of Gram-negative bacteria, and is involved in several processes among which cell division (15, 16). In agreement to this, another recent study showed that, at least for the serine chemoreceptor Tsr, the Tol-Pal complex together with the nucleoid are required for polar localization, and that nucleoid exclusion is a driving force for polar localization of MCPs (17). Here, we evaluated the different polar localization models in *E. coli* using the aspartate chemoreceptor Tar. We found neither evidence for periodic clustering nor for nucleoid exclusion, but both membrane curvature and the Tol-Pal system appeared to be required for polar localization of Tar in *E. coli*.

Results

Stochastic nucleation

The stochastic nucleation model has been based on the formation of large YFP-CheR and CheY-YFP clusters that were regularly spaced with a periodicity of approximately 1 µm (5). To confirm that MCPs also produce these regular clusters, the *E. coli* chemoreceptor Tar was C-terminally fused with a monomeric GFP variant (mGFP). Since GFP tends to form weak dimers, monomeric GFP was chosen to prevent possible localization artefacts (18). To reduce potential artefacts related to protein overexpression, a low copy plasmid with a weakened IPTG-inducible promoter (pTRC99A (19)) was used to express the fusion protein. As shown in Fig. 1A, Tar-mGFP shows a classical septal and polar localization pattern. This localization does not depend on interaction with other chemoreceptors, since expression of the fusion protein in a MCP deletion strain shows the same localization pattern (Fig. S2C). The Tar-mGFP fusion protein was active according to a swarming plate assay (14) (Fig. S1). The expression level was approximately twice that of Tar-mGFP expressed from its native promoter, but this increased expression did not change the localization pattern (Fig. S2). We noticed that the use of the native promoter resulted in a substantial variation in expression levels between cells, and therefore we continued with the IPTG-inducible construct.

According to the stochastic nucleation model, chemotaxis proteins form large protein clusters prior to the initiation of cell division. To determine at what time in the cell cycle Tar accumulates at midcell, we performed a virtual time lapse approach by sorting cells on size (Fig. 1A, lower panel), and plotting the related fluorescence intensities and cell constriction (Fig. 1C) (20). As a timer for cell division, we followed the localization of GFP-labelled FtsN, an essential cell division protein and part of the cell division machinery (21) (Fig. 1B). Comparison of the localization profiles indicates that Tar appears later at midcell compared to FtsN, suggesting that clustering of the chemotaxis proteins does not precede recruitment of FtsN (or the division machinery). To further confirm this, we co-stained FtsZ and FtsN in cells expressing Tar-mGFP using immunofluorescence (Fig. S3). This double labelling

experiment clearly showed that Tar-mGFP accumulated at midcell after FtsZ and FtsN.

To determine whether Tar forms regularly spaced clusters with a periodicity of around 1 µm in filamentous non-dividing cells, we blocked cell division using the antibiotic cephalexin, which inactivates the cell division protein FtsI required for septum synthesis (22). As shown in Fig. 2A & B, no large regularly spaced fluorescent clusters were observed along the lateral wall of filamentous cells, but the polar clustering remained. Based on these data it seems unlikely that Tar uses stochastic clustering to accumulate at cell poles.

Nucleoid exclusion

In a recent report it was suggested that the serine MCP Tsr of *E. coli* is also driven to cell poles by the 'volume exclusion' effect of the nucleoid (17). To examine whether nucleoids influence the distribution of Tar, we stained the cephalexin treated cells with the fluorescence DNA dye DAPI to visualize the nucleoids (Fig. 2B). We could not detect any correlation with the position of the nucleoids and the density of Tar-mGFP clusters along the lateral wall (see also line scans in Fig. 2B, and Fig. S4). To corroborate this, cells were treated with ciprofloxacin, which inhibits DNA gyrase and blocks DNA replication, resulting in a dense nucleoid at the centre of long cell, since the activated SOS-response also inhibit cell division (Fig. 2C) (23, 24). Also under these conditions the Tar-mGFP signal was not reduced at the area occupied by the nucleoid. Thus, at least for Tar, nucleoid exclusion does not seem to be important for polar localization.

CheA stimulated clustering

Interaction of MCP trimer-of-dimers is stimulated by dimerization of the kinase CheA, which binds to the cytoplasmic termini of MCP trimers (2). In fact, we have found that CheA is essential to maintain polar localization of the chemoreceptor TlpA in *B. subtilis* (13). However, it has been shown some time ago that in *E. coli* CheA is not necessary for the polar clustering of chemoreceptor (25). Indeed, when we expressed Tar-mGFP in a *cheA* deletion mutant background, the protein accumulated at midcell and cell poles (Fig. 3A).

There is some delay in midcell accumulation of Tar-mGFP compared to wild type cells (compare with Fig. 1A, and Fig. S3 & S5). This is likely due to reduced clustering of MCP trimers, and consequently, decreased retention of trimers at midcell.

Role of Tol-Pal

The trans-envelope Tol-Pal complex, which accumulates at midcell and assist in the division of the outer cell membrane (16), has been shown to be required for the polar localization of chemoreceptor proteins, and pulldown experiments suggested an interaction between TolA and chemoreceptors (14). To verify this, we expressed the Tar-mGFP fusion in a *pal* deletion mutant. Indeed, the polar accumulation of the fusion protein was completely abolished, however, there was still a strong accumulation at midcell (Fig. 3B). When the fusion protein was expressed in a *tolA* deletion mutant, a similar localization pattern was observed (Fig. S6).

During cell division, the cell membrane will cover the nascent division septum, thereby creating two flat membranes in close proximity between daughter cells. This will give a higher fluorescent membrane signal at midcell, so even when Tar is unable to localize and diffuses freely throughout the cell membrane, the extra cell membranes at the division sites could, in theory, account for an increase in GFP signal at midcell. To assess this, we followed the localization of a general transmembrane protein, the glycerol-3-phosphate transporter GlpT (26), throughout the cell cycle in the *pal* mutant. Indeed, the GFP signal showed a slight accumulation at midcell when cells started to divide (Fig. 3C), however, the signal intensity was much lower compared to that of Tar-mGFP (Fig. 3D), indicating that the double cell membrane at the division site is not responsible for the strong fluorescence Tar-mGFP signal at midcell in *tol-pal* mutant cells.

Membrane curvature

A closer inspection of the *pal* mutant revealed that the Tar-mGFP signal often appears as two fluorescent dots at midcell (Fig. 3B), suggesting that Tar accumulates as a ring at

midcell at the base of the nascent septum. We never observed Tar-mGFP signals of smaller sizes at midcell, reminiscent to constricting Z-rings, indicating that the fusion protein does not follow the leading edge of the ingrowing septum. The Tol-Pal complex is recruited to the division site, and links invagination of the outer membrane with that of the cell membrane during cell division (16). Inactivation of Tol-Pal delays invagination of the outer membrane and cell separation, resulting in the formation of a division septum that resembles the septal cross walls in Gram-positive bacteria (27). The consequence of such mode of division is that the cell membrane at the transition from the lateral wall to the nascent septal wall is strongly curved (28). This is where the Tar-mGFP fluorescent signal seems to accumulate in the *pal* deletion mutant (Fig. 3B). Presumably, Tar localizes at this region because of the curvature mismatch generated by the tripod configuration of the trimer-of-dimers in combination with the stiffness of the dimers (29). Tension in the membrane is released when these tripods locate to regions of the cell with a corresponding membrane curvature, such as those found at cell division sites. To confirm this, we introduced a N379R mutation in the trimerization site of Tar, corresponding to the N381R mutation in Tsr, which has been shown to abolish trimerization (30). Since single membrane spanning MCP dimers will not deform the membrane, they should therefore not accumulate at cell division sites when membrane curvature is the main driver for localization (Fig. 4A). Indeed, the N379R mutation resulted in the absence of a clear septal and polar fluorescent signal (Fig. 4B). When we increased the flexibility of the dimers by introducing two glycines at position 249 and 250, creating a stretch of 3 glycines in the HAMP domain (G248G D249G L250G), Tar was also no longer able to accumulate at midcell and cell poles (Fig. 4C & D), in line with the assumption that the unstructured glycine stretch eliminates the membrane curvature preference of the trimer (Fig. 4A) (12, 13). This delocalization was not a consequence of protein degradation, since Western blot analysis indicated that the point mutations did not affect stability of the Tar-mGFP fusions (Fig. S7). Finally, when the dimerization and HAMP domain mutants were expressed in a *pal* mutant a comparable delocalization was observed (Fig. S8). Thus, membrane curvature at the division septum seems to drive the localization of Tar trimers-of-

196 dimers.

Discussion

Our data suggests that the MCPs of *E. coli* and *B. subtilis* arrive at cell poles by a comparable mechanism that begins with cell division. First, they accumulate at midcell where the cell membrane is bend inwards and strongly curved due to synthesis of the nascent cell division septum. Based on a composite crystal structure the curvature of one trimer-of-dimers was calculated to amount to a radius of approximately 37 nm (8). Therefore, the membrane curvature mismatch is reduced considerably when a trimer-of-dimers is located at the base of the nascent division septum. After septation is completed, *B. subtilis* chemoreceptor clusters are maintained at the newly formed poles by forming large protein clusters that require CheA. However, in *E. coli*, the Tol-Pal complex is required to keep chemoreceptors clustered at the newly formed cell poles, instead of CheA. Co-immunoprecipitation experiments have suggested an interaction between this complex and chemoreceptor proteins (14). Since lateral diffusion of the large trans-envelope Tol-Pal complex is likely to be hampered by the peptidoglycan layer, interactions between Tol-Pal and chemoreceptor proteins might anchor MCPs and maintain their polar localization.

Several papers have argued that the curvature of the *E. coli* cell pole is sufficient to attract MCP trimers (8, 12, 31). However, the polar localization of Tar-mGFP is completely abolished when Tol-Pal is absent. This indicates that the curvature at the cell pole is not sufficient to markedly reduce the membrane curvature mismatch created by the Tar trimer-of-dimers. This is maybe not so surprising since the cell pole has a curvature with a radius of approximately 500 nm, which is much larger compared to the 37 nm radius of MCP trimer-of-dimers (8). Moreover, the cylindrical lateral wall has a radius that is comparable to that of the cell pole, which makes the perceived curvature increase of cell poles even smaller.

Over the years different mechanisms have been postulated and contradictory results have been obtained in the research of polar localization of *E. coli* chemoreceptors. One possible explanation is that different groups use different protein reporters for chemoreceptors. In many studies, the cytoplasmic CheR has been used as a proxy for

chemoreceptor clusters (5, 12, 14), while others have looked directly at the localization of MCPs (17). Another reason might be the use of fluorescent protein reporters with a tendency to dimerize, such as YFP and GFP. This characteristic has been shown to cause localization artefacts, especially when used with proteins that form multimers (18). Finally, we cannot exclude that different chemoreceptor use different mechanisms for localization. Nevertheless, both in *E. coli* and in *B. subtilis* it appears that the strong curvature generated during cell division is a key driving force for the localization of MCPs.

Materials and methods

Bacterial strains and growth conditions

All strains used in this study are listed in Table S1. Strains were grown in GB1 minimal medium (6.33 g/l $K_2HPO_4.3H_2O$, 2.95 g/l KH_2PO_4, 1.05 g/l $(NH_4)_2SO_4$, 0.10 g/l $MgSO_4.7H_2O$, 28 mg/l $FeSO_4.7H_2O$, 7.10 mg/l $Ca(NO_3)_2.4H_2O$) supplemented with vitamin B1 (4 mg/ml) and 0.4 % glucose as carbon-source, as previously described (32, 33). Auxotrophic BW25113 cells required arginine (50 µg/ml), glutamine (50 µg/ml), uracil (20 µg/ml), and thymidine (2 µg/ml). Either 100 µg/ml (or 5 µg/ml in cases of *pal* or *tolA* mutant) of ampicillin was added to the growth medium to maintain plasmids.

Plasmid construction

Purified DNA amplicons were used in a 1:10 molar ratio of vector to insert(s) in Gibson Assembly reaction (20 µl) at 50^{o}C for 60 minutes. 5 µl of each Gibson Assembly reaction mix was used to transform ultra-competent *E. coli* TOP 10 cells. Ultra-competent *E. coli* TOP 10 cells were prepared as described in Hanahan *et al.* (34). Plasmids were sequenced to confirm constructs. Plasmids were transformed into chemically competent BW23115 wild type or mutant cells, prepared as described in Maniatis et al. (35). Transformants were selected on selective LB agar plates containing the appropriate concentration of antibiotic. Oligos (Table S3) and plasmids (Table S2) used in this study are listed in the supplementary information.

To construct Tar-mGFP fusion, the point mutation GFP(A206K) was introduced in plasmid pBAD24-Tar-GFP (36) to prevent dimerization of GFP (18). The mutation was made by quick change using primer pair GFP(A206K)-for/GFP(A206K)-rev, resulting in plasmid pBAD24-Tar-mGFP. To express Tar-mGFP from a weakened isopropyl ß-D-thiogalactoside (IPTG)-inducible promoter (19) and low copy number plasmid, the pBAD promoter was replaced by the pTRC99A promoter from pSAV57 (32), and the pUC19ori was replaced with the pSC101 ori from pSEN29 (37). First, pBAD24-Tar-mGFP was linearized by PCR

amplification using primer pair TerS327/TerS328, then the pSC101 origin was amplified with primer pair TerS425/TerS426, and subsequently both products were ligated by Gibson Assembly (38), resulting in plasmid pTNV107 (pBAD24-Tar-mGFP-pSC101 ori). To obtain the weak IPTG-inducible low copy number plasmid, plasmid pTNV107 was linearized with primer pair TerS425/TerS507, and the pTRC99A promoter was amplified from pSAV057 using primer pair TerS328/TerS506. The products were ligated using Gibson Assembly, resulting in pTNV149 (pTRC99A-Tar-mGFP-pSC101 ori). To express Tar-mGFP using native promoter from the same low copy number plasmid, the pBAD promoter in plasmid pTNV107 was replaced with the native promoter of *tar.* To this end, pTNV107 was linearized with primer pair TerS457/TerS508, and a fragment of *tar* including its promoter (39) was amplified from genomic DNA using primer pair TerS509/TerS510. The products were ligated using Gibson Assembly, resulting in pTNV148 (P*tar*-Tar-mGFP pSC101 ori).

To test if curvature caused by trimer-of-dimers is essential for Tar-mGFP localization, we introduced a N379R point mutation in Tar that abolishes the interaction between dimers. The primer sets TerS328/TerS517 and TerS425/457 were used to introduce N379R in pTNV149 (pTRC99A-Tar-mGFP-pSC101 ori) using Gibson Assembly, resulting in plasmid pTNV154 (pTRC99A-Tar(N379R)-mGFP-pSC101 ori). We also introduced a stretch of 3-glycines in the HAMP domain of Tar to make the dimers flexible. Primer pairs TerS328/TerS516 and TerS425/515 were used to introduce G248G D249G L250G in Tar in pTNV149 (pTRC99A-Tar-mGFP-pSC101 ori), resulting in plasmid pTNV153 ((pTRC99A-Tar(G248G D249G L250G-mGFP-pSC101 ori).

To compare midcell localization of Tar-mGFP to divisome assembly, we used the late cell division protein FtsN fused to monomeric GFP. The mGFP-FtsN fusion was constructed by PCR amplification of pTNV149 with primer pair TerS418/520, a monomeric variant of *gfp* from pTNV100 with primer pair TerS362/521, and *ftsN* from *E. coli* genomic DNA with primer pair TerS523/541 followed by Gibson Assembly, resulting in plasmid pTNV155 (pTRC99A- mGFP-FtsN-pSC101 ori).

As a control for membrane localization, we constructed a glycerol-3-phosphate

transporter GlpT-GFP fusion. mGFP-GlpT was made by PCR amplification of pTNV149 with primer pair TerS418/520, a monomeric variant of *gfp* from pTNV100 with primer pair TerS362/521, and *glpT* from *E. coli* genomic DNA with primer pair TerS544/545, followed by Gibson Assembly, resulting in plasmid pTNV162 (pTRC99A- mGFP-GlpT-pSC101 ori).

Functionality and stability of Tar-mGFP fusions

To test whether the Tar-mGFP fusions are functional we performed a motility swarming experiment according to Santos et *al* (14). The motility of Δ*mcp* cells expressing the wild type and mutant Tar fusions was tested by spotting 10 µl of culture with a comparable OD_{600} of ~0.5 on LB plates containing 0.25% agar including 15 µM IPTG for the plasmid containing strains.

To check that the Tar-mGFP mutant proteins were not degraded, we performed a western blot analysis using GFP antibody. The relevant strains were grown and expression of the fusion protein was induced with 15 µM IPTG for two hours. After correction for optical density, cells were boiled in Laemmli sample buffer for 15 minutes. 15 µl of each sample were used for SDS-PAGE.

Microscopy and image analysis

The virtual time lapse is based on the fact that during steady state growth the average mass of all cells and their age frequency distribution are constant allowing precise spatio-temporal information on protein localization during the cell cycle, as described in (40). Steady state was obtained by growing cells in GB1 medium at 30 ^{o}C under shaking (210 rpm) while keeping OD_{450} below 0.2 by regular dilution in pre-warmed medium for three days to reach steady state growth. At steady state, Tar-mGFP was induced with 15 µM of IPTG for at least two-doubling times. Steady-state cells were centrifuged at 1000 RPM for 2 minutes to bring the OD_{450} to ~0.4.

0.3 µl cells were spotted onto a microscope slide covered with a thin layer of 1.3% agarose. When applicable, cells were treated with 15 µg/ml cephalexin for 1 to 4 h, or 0.035

μg/ml ciprofloxacin for 1 h. The presence of the *bla* gene, encoding beta-lactamase, on the plasmids did not interfere with the activity of the beta-lactam antibiotic cephalexin. Images were acquired with 500 ms exposure time for the GFP channel. Fluorescent microscopy was carried out with a Nikon Eclipse Ti equipped with a CFI Plan Intensilight HG 130 W lamp, a C11440-22CU Hamamatsu ORCA camera, and NIS elements software, version 4.20.01. Images were analysed using Image J v 1.50i (https://imagej.nih.gov/ij/) and the Image J plugin ObjectJ version 03p (40).

To construct the localization profiles of the fluorescent signals, images were analysed using Coli-Inspector in the advanced mode (40). First, phase contrast and fluorescent channels were aligned using the accompanying macro, then the background of the fluorescent channels were subtracted using the built-in command of Coli-Inspector. Secondly, individual cells were selected and manually confirmed. Finally, selected cells were sorted on length and the related fluorescent signal along the cell axis was also obtained.

Immunofluorescence labelling of FtsZ and FtsN

Immunofluorescence staining of FtsZ and FtsN was performed as described before (40). Briefly, 12.2 ml of cells were fixed with 2.8% formaldehyde and 0.04% glutaraldehyde for 15 minutes. Cells were harvested by centrifugation, washed and resuspended in 150 µl PBS buffer. To permeabilize the cells, the fixed cells were treated with 0.1% Triton X-100/PBS at room temperature for 45 minutes followed by a triple washing step with PBS. Cells were then treated with 100 µg/ml lysozyme and 5 mM EDTA at room temperature for 45 minutes, and subsequently washed 3x with PBS. Prior to labelling, non-specific binding sites were blocked by incubating cells in 0.5% (w/v) blocking reagents (F. Hoffmann-La Roche) in PBS at 37 ^{o}C for 30 minutes. FtsZ and FtsN were immune-labelled using purified primary polyclonal antibodies against each protein (40), diluted in 1:500 blocking buffer for an hour at 37 ^{o}C. Cells were washed 3x with PBS and subsequently incubated with secondary donkey-α-rabbit-CY3 antibody diluted 1:600 in blocking buffer at 37 ^{o}C for 30 minutes. Cells were washed 3x with PBS/0.05% Tween-20, and once with PBS and after resuspension in PBS

345 stored in the fridge, ready for immunofluorescence microscopy.

Acknowledgements

We thank the members of the Bacterial Cell Biology group for useful discussions, especially Tanneke den Blaauwen for discussions on protein localization in *E. coli* and for providing antibodies against FtsZ and FtsN. We would like to thank Séverin Ronneau (Imperial College London) for constructing the initial monomeric GFP reporter, and Ikuro Kawagishi (Hosei University), Joen Luirink (VU University), Pierre Genevaux (CNRS), and Tom Shimizu (AMOLF) for kindly providing us with strains and plasmids. This research was funded by a Biotechnology and Biological Sciences Research Council (BBSRC) grant BB/I01327X/1, Marie Curie CIG grant DIVANTI (618452), and NWO STW-Vici grant 12128.

References

1. **Porter SL**, **Wadhams GH**, **Armitage JP**. 2011. Signal processing in complex chemotaxis pathways. Nat Rev Micro **9**:153–165.

2. **Parkinson JS**, **Hazelbauer GL**, **Falke JJ**. 2015. Signaling and sensory adaptation in *Escherichia coli* chemoreceptors: 2015 update. Trends in Microbiology **23**:257–266.

3. **Alley MRK**, **Maddock JR**, **Shapiro L**. 1992. Polar localization of a bacterial chemoreceptor. Genes Dev **6**:825–836.

4. **Maddock**, **Shapiro L**. 1993. Polar location of the chemoreceptor complex in the *Escherichia coli* cell. Science **259**:1717–1723.

5. **Thiem S**, **Kentner D**, **Sourjik V**. 2007. Positioning of chemosensory clusters in *E. coli* and its relation to cell division. EMBO J **26**:1615–1623.

6. **Thiem S**, **Sourjik V**. 2008. Stochastic assembly of chemoreceptor clusters in *Escherichia coli*. Mol Microbiol **68**:1228–1236.

7. **Greenfield D**, **McEvoy AL**, **Shroff H**, **Crooks GE**, **Wingreen NS**, **Betzig E**, **Liphardt J**. 2009. Self-organization of the *Escherichia coli* chemotaxis network imaged with super-resolution light microscopy. PLOS Biol **7**:e1000137.

8. **Endres RG**. 2009. Polar chemoreceptor clustering by coupled trimers of dimers. Biophysical Journal **96**:453–463.

9. **Kim KK**, **Yokota H**, **Kim S-H**. 1999. Four-helical-bundle structure of the cytoplasmic domain of a serine chemotaxis receptor. Nature **400**:787–792.

10. **Derganc J**. 2007. Curvature-driven lateral segregation of membrane constituents in Golgi cisternae. Phys Biol **4**:317–324.

11. **Aimon S**, **Callan-Jones A**, **Berthaud A**, **Pinot M**, **Toombes GES**, **Bassereau P**. 2014. Membrane Shape Modulates Transmembrane Protein Distribution. Dev Cell **28**:212–218.

12. **Draper W**, **Liphardt J**. 2017. Origins of chemoreceptor curvature sorting in *Escherichia coli*. Nat Commun **8**:14838.

13. **Strahl H**, **Ronneau S**, **González BS**, **Klutsch D**, **Schaffner-Barbero C**, **Hamoen LW**. 2015. Transmembrane protein sorting driven by membrane curvature. Nat Commun **6**:8728.

14. **Santos TMA**, **Lin T-Y**, **Rajendran M**, **Anderson SM**, **Weibel DB**. 2014. Polar localization of *Escherichia coli* chemoreceptors requires an intact Tol-Pal complex. Mol Microbiol **92**:985–1004.

15. **Sturgis JN**. 2001. Organisation and evolution of the tol-pal gene cluster. J Mol Microbiol Biotechnol **3**:113–122.

16. **Gerding MA**, **Ogata Y**, **Pecora ND**, **Niki H**, **de Boer PAJ**. 2007. The trans-envelope Tol-Pal complex is part of the cell division machinery and required for proper outer-membrane invagination during cell constriction in *E. coli*. Mol Microbiol **63**:1008–1025.

17. **Neeli-Venkata R**, **Startceva S**, **Annila T**, **Ribeiro AS**. 2016. Polar Localization of the Serine Chemoreceptor of *Escherichia coli* Is Nucleoid Exclusion-Dependent. Biophysical Journal **111**:2512–2522.

18. **Landgraf D**, **Okumus B**, **Chien P**, **Baker TA**, **Paulsson J**. 2012. Segregation of molecules at cell division reveals native protein localization. Nat Meth **9**:480–482.

19. **Amann E**, **Ochs B**, **Abel KJ**. 1988. Tightly regulated tac promoter vectors useful for the expression of unfused and fused proteins in *Escherichia coli*. Gene **69**:301–315.

20. **Blaauwen Den T**, **Buddelmeijer N**, **Aarsman M**, **Hameete CM**, **Nanninga N**. 1999. Timing of FtsZ assembly in *Escherichia coli*. Journal of Bacteriology **181**:5167–5175.

21. **Addinall SG**, **Cao C**, **Lutkenhaus J**. 1997. FtsN, a late recruit to the septum in *Escherichia coli*. Mol Microbiol **25**:303–309.

22. **Botta GA**, **Park JT**. 1981. Evidence for involvement of penicillin-binding protein 3 in murein synthesis during septation but not during cell elongation. Journal of Bacteriology **145**:333–340.

23. **LeBel M**. 1988. Ciprofloxacin: Chemistry, Mechanism of Action, Resistance, Antimicrobial Spectrum, Pharmacokinetics, Clinical Trials, and Adverse Reactions. Pharmacotherapy: The Journal of Human Pharmacology and Drug Therapy **8**:3–30.

24. **Khodursky AB**, **Cozzarelli NR**. 1998. The mechanism of inhibition of topoisomerase IV by quinolone antibacterials. Journal of Biological Chemistry **273**:27668–27677.

25. **Skidmore JM**, **Ellefson DD**, **McNamara BP**, **Couto MMP**, **Wolfe AJ**, **Maddock JR**. 2000. Polar clustering of the chemoreceptor complex in *Escherichia coli* occurs in the absence of complete CheA function. Journal of Bacteriology **182**:967–973.

26. **Oswald F**, **Varadarajan A**, **Lill H**, **Peterman EJG**, **Bollen YJM**. 2016. MreB-Dependent Organization of the *E. coli* Cytoplasmic Membrane Controls Membrane Protein Diffusion. Biophysical Journal **110**:1139–1149.

27. **Meury J**, **Devilliers G**. 1999. Impairment of cell division in *tolA* mutants of *Escherichia coli* at low and high medium osmolarities. Biol Cell **91**:67–75.

28. **Lenarcic R**, **Halbedel S**, **Visser L**, **Shaw M**, **Wu LJ**, **Errington J**, **Marenduzzo D**, **Hamoen LW**. 2009. Localisation of DivIVA by targeting to negatively curved membranes. EMBO J **28**:2272–2282.

29. **Kim S-H**, **Wang W**, **Kim KK**. 2002. Dynamic and clustering model of bacterial chemotaxis receptors: Structural basis for signaling and high sensitivity. Proc Natl Acad Sci USA **99**:11611–11615.

30. **Gosink KK**, **Zhao Y**, **Parkinson JS**. 2011. Mutational analysis of N381, a key trimer contact residue in Tsr, the *Escherichia coli* serine chemoreceptor. Journal of Bacteriology **193**:6452–6460.

31. **Haselwandter CA**, **Wingreen NS**. 2014. The role of membrane-mediated interactions in the assembly and architecture of chemoreceptor lattices. PLoS Comput Biol **10**:e1003932.

32. **Alexeeva S**, **Gadella TWJ**, **Verheul J**, **Verhoeven GS**, **Blaauwen den T**. 2010. Direct interactions of early and late assembling division proteins in *Escherichia coli* cells resolved by FRET. Mol Microbiol **77**:384–398.

33. **Aarsman MEG**, **Piette A**, **Fraipont C**, **Vinkenvleugel TMF**, **Nguyen Distèche M**, **Blaauwen den T**. 2005. Maturation of the *Escherichia coli* divisome occurs in two steps. Mol Microbiol **55**:1631–1645.

34. **Hanahan D**, **Jessee J**, **Bloom FR**. 1991. Plasmid Transformation of *Escherichia coli* and Other Bacteria. Methods Enzymol **204**:63–113.

35. **Sambrook J**, **Maniatis T**. 1989. Molecular Cloning. Cold Spring Harbor Laboratory Press.

36. **Shiomi D**, **Yoshimoto M**, **Homma M**, **Kawagishi I**. 2006. Helical distribution of the bacterial chemoreceptor via colocalization with the Sec protein translocation machinery. Mol Microbiol, 2nd ed. **60**:894–906.

37. **Genevaux P**, **Keppel F**, **Schwager F**, **Langendijk-Genevaux PS**, **Hartl FU**, **Georgopoulos C**. 2004. In vivo analysis of the overlapping functions of DnaK and trigger factor. EMBO Rep **5**:195–200.

38. **Gibson DG**, **Young L**, **Chuang R-Y**, **Venter JC**, **Hutchison CA**, **Smith HO**. 2009. Enzymatic assembly of DNA molecules up to several hundred kilobases. Nat Meth **6**:343–345.

39. **Kundu TK**, **Kusano S**, **Ishihama A**. 1997. Promoter selectivity of *Escherichia coli* RNA polymerase sigmaF holoenzyme involved in transcription of flagellar and chemotaxis genes. Journal of Bacteriology **179**:4264–4269.

40. **Vischer NOE**, **Verheul J**, **Postma M**, **van den Berg van Saparoea B**, **Galli E**, **Natale P**, **Gerdes K**, **Luirink J**, **Vollmer W**, **Vicente M**, **Blaauwen den T**. 2015. Cell age dependent concentration of *Escherichia coli* divisome proteins analyzed with ImageJ and ObjectJ. Front Microbiol **6**:586.

Figure legends

Fig. 1. Localization of Tar-mGFP

(A) Fluorescence microscopy image of wild type *E. coli* cells expressing Tar-mGFP. Lower panel shows sorted axial fluorescence profiles, indicative for Tar-mGFP localization during the cell cycle. (B) Fluorescence microscopy image and cell cycle localization profile of cells expressing mGFP-FtsN. (C) Graphical presentation of cell constriction and fluorescence signals during the cell cycle calculated from the localization profiles. Age refers to age classes divided in 5% (cell cycle) bins, see Material and Methods for details. 5074 and 6437 cells were used to construct the cell cycle localization profiles for mGFP-FtsN and Tar-mGFP, respectively. Scale bars are 2 µm. Strains used in A and B are TSE29 and TSE48, respectively.

Fig. 2. Tar-mGFP clustering and relation to nucleoid position

(A) Fluorescence microscopy image and localization profile of Tar-mGFP expressing cells treated with 15 µg/ml cephalexin for 1 h. 1872 cells were used to construct the localization profile. (B) Fluorescence microscopy image of Tar-mGFP expressing cells treated with 15 µg/ml cephalexin for 3 h. Nucleoids were stained with DAPI. Line scans for the GFP and DAPI signals are presented below. More examples are shown in Fig. S4. (C) Fluorescence microscopy image of Tar-mGFP expressing cells treated with 0.035 µg/ml ciprofloxacin for 1 h. Nucleoids were stained with DAPI. Scale bars are 2 µm. Strain used is TSE29.

Fig. 3. Effect of *cheA* and *pal* deletion mutant on Tar-mGFP localization

(A) Fluorescence microscopy image and localization profile of Tar-mGFP expressing *cheA* deletion mutant. 5948 cells were used to construct the localization profile. (B) Fluorescence microscopy image and localization profile of Tar-mGFP expressing *pal* deletion mutant. Arrow indicates Tar-mGFP foci. 9044 cells were used to construct the localization profile. (C) Fluorescence microscopy image and localization profile of mGFP-GlpT expressed in the *pal*

deletion mutant. 5214 cells were used to construct the localization profile. (D) Graphical presentation of fluorescence signals during the *pal* deletion mutant cell cycle calculated from the localization profiles. Age refers to age classes divided in 5% (cell cycle) bins. Scale bars are 2 µm. Strains used in A, B and C are TSE38, TSE31 and TSE71, respectively.

Fig. 4. Membrane curvature is important for localization

(A) Schematic presentation of the effect of dimerization mutation N379R and the triple glycine substitution (G248G D249G L250G) on membrane curvature mismatch. (B) Fluorescence microscopy image and localization profile of Tar(N379R)-mGFP expressing cells. 7331 cells were used to construct the localization profile. (C) Fluorescence microscopy image and localization profile of Tar(G248G D249G L2450G)-mGFP expressing cells. 7856 cells were used to construct the localization profile. (D) Graphical presentation of fluorescence signals during the cell cycle calculated from the localization profiles. Tar-mGFP panel is the same as in figure 1C. Age refers to age classes divided in 5% (cell cycle) bins. Scale bars are 2 µm. Used strains in B and C are TSE42 and TSE41, respectively, and in D strains TSE29, TSE42, TSE41 and TSE67, respectively.

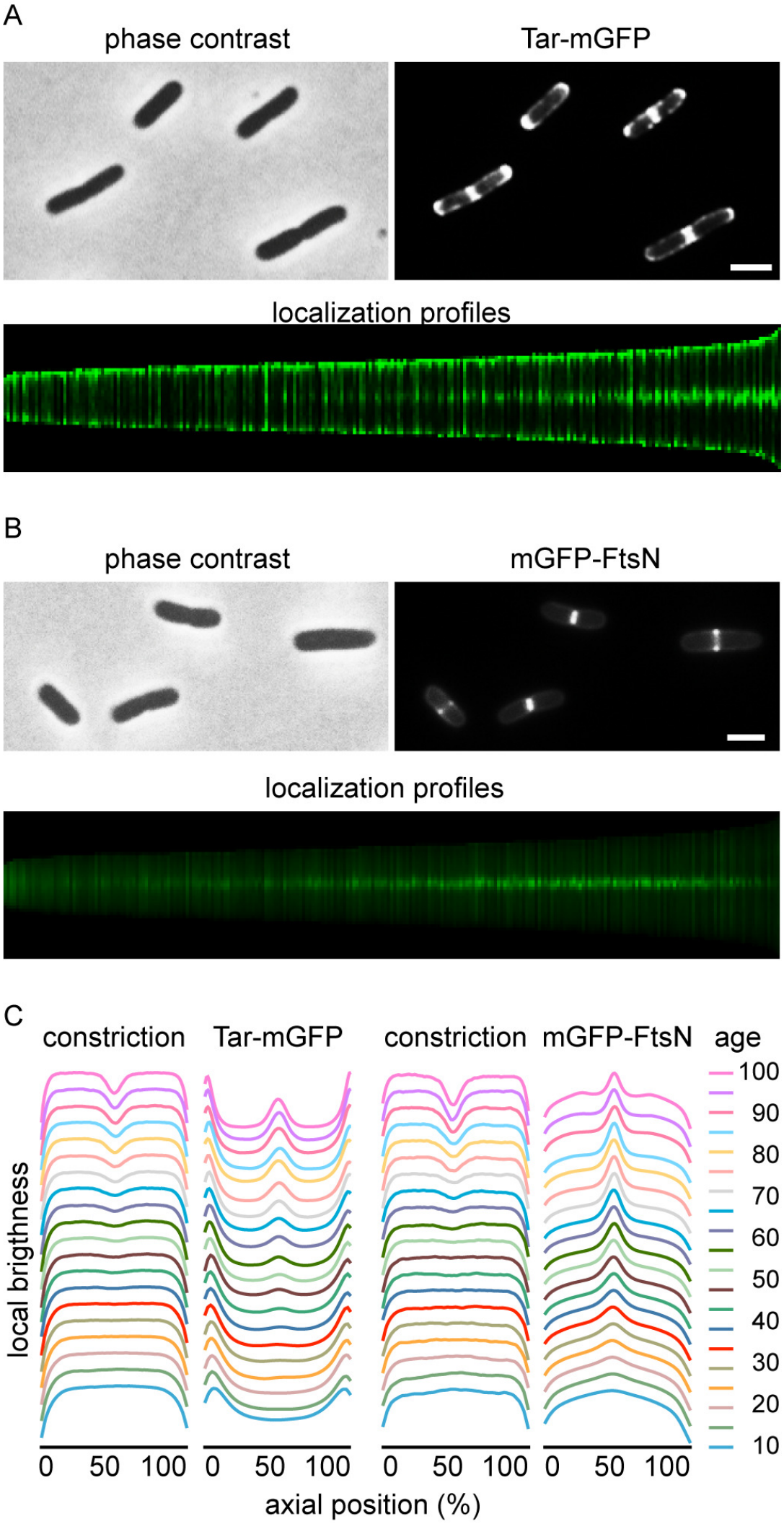
A
phase contrast
Tar-mGFP
localization profiles
B
phase contrast
mGFP-FtsN
localization profiles
C
constriction
Tar-mGFP
constriction
mGFP-FtsN
age
100
90
80
70
60
50
40
30
20
10
local brigthness
0
50
100
0
50
100
0
50
100
0
50
100
axial position (%)

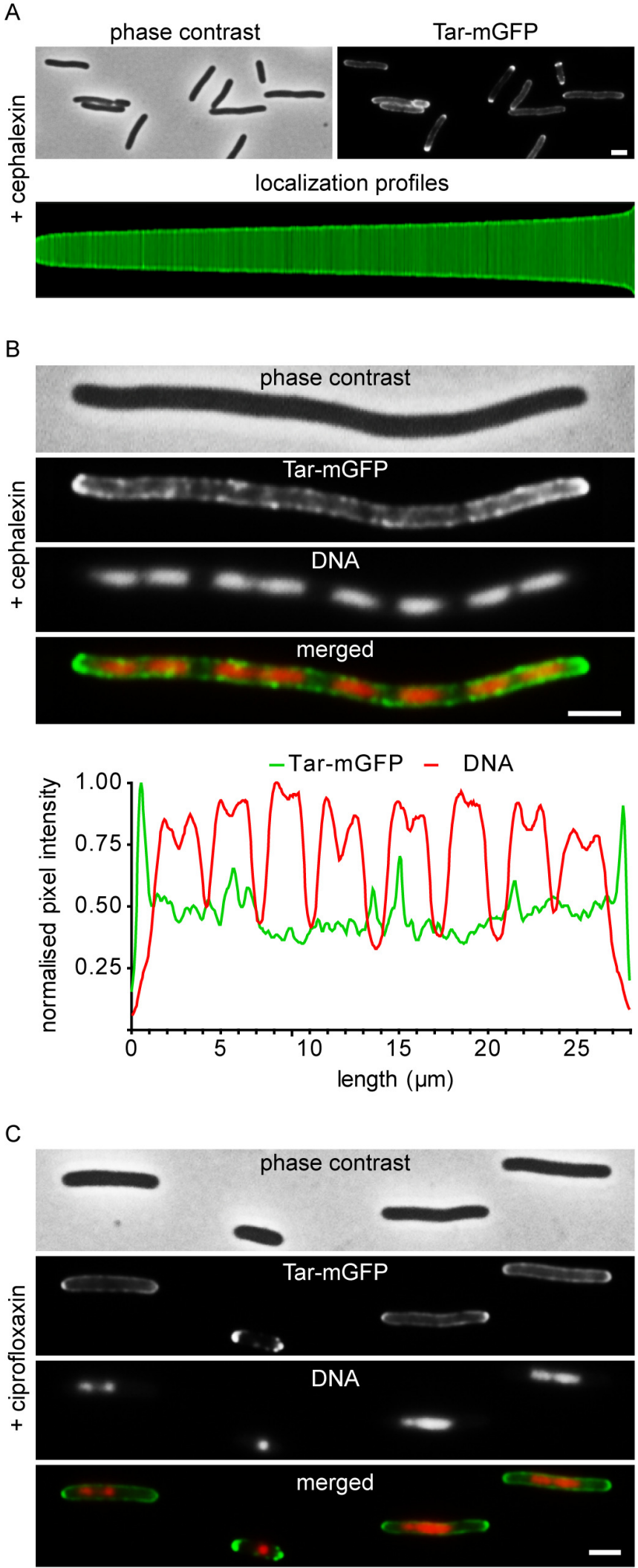
A
phase contrast
Tar-mGFP
+ cephalexin
localization profiles
B
phase contrast
Tar-mGFP
+ cephalexin
DNA
merged
Tar-mGFP
DNA
normalised pixel intensity
1.00
0.75
0.50
0.25
0
5
10
15
20
25
length (μm)
C
phase contrast
Tar-mGFP
+ ciprofloxaxin
DNA
merged

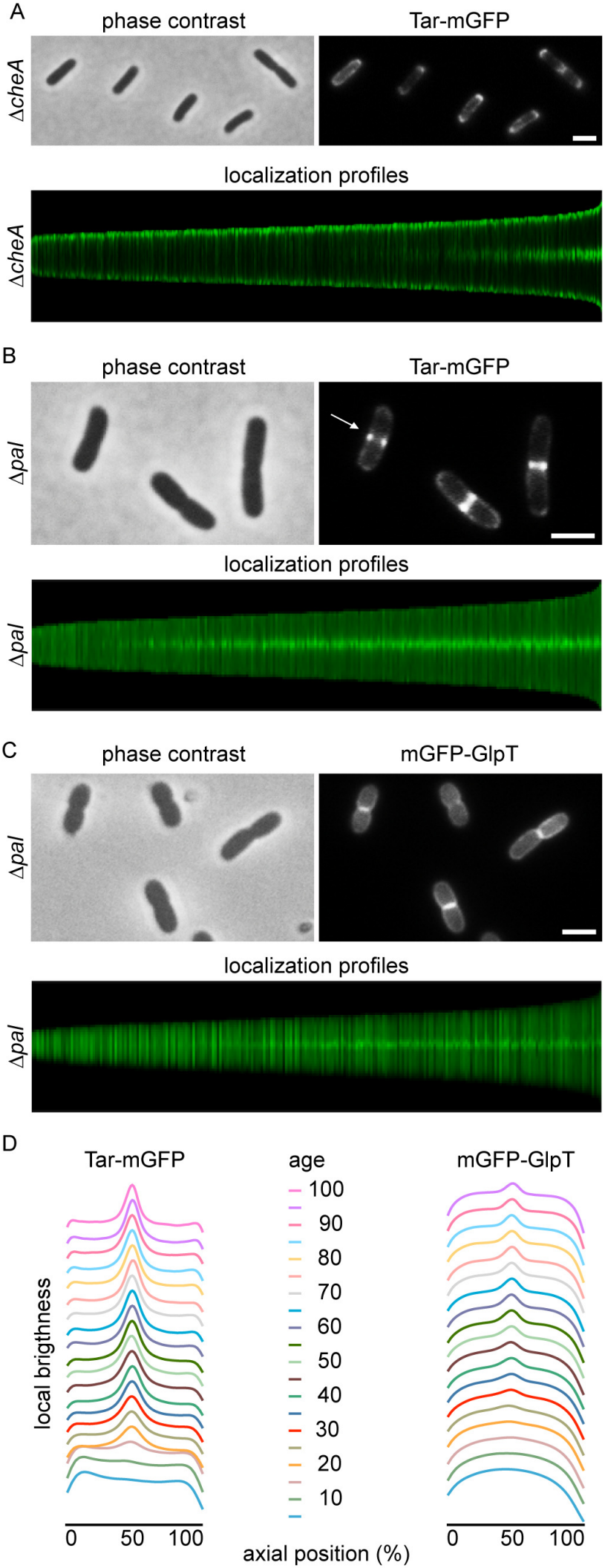
A
phase contrast
Tar-mGFP
ΔcheA
localization profiles
ΔcheA
B
phase contrast
Tar-mGFP
Δpal
localization profiles
Δpal
C
phase contrast
mGFP-GlpT
Δpal
localization profiles
Δpal
D
Tar-mGFP
age
mGFP-GlpT
100
90
80
70
60
50
40
30
20
10
local brigthness
0
50
100
0
50
100
axial position (%)

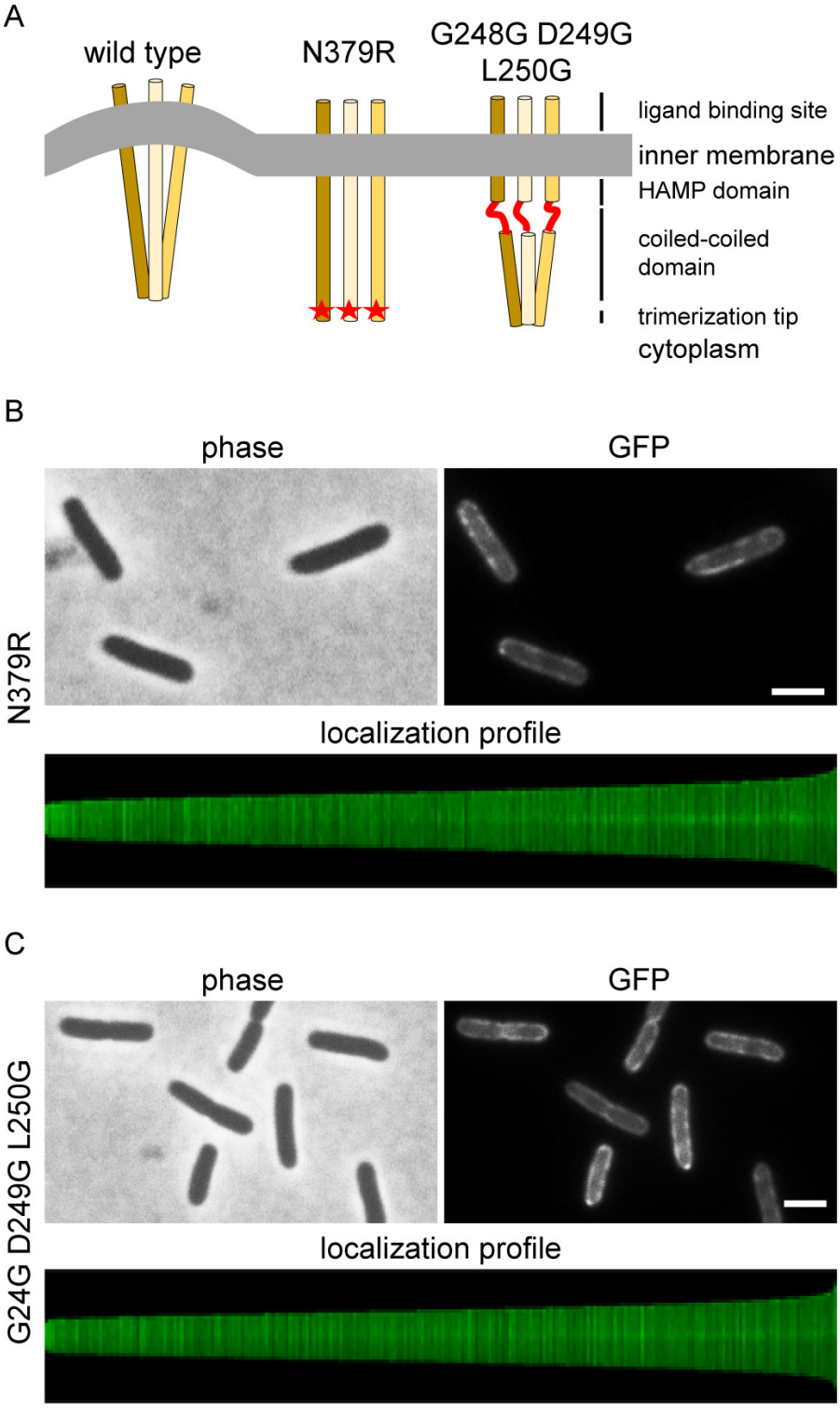
A
wild type
N379R
G248G D249G
L250G
ligand binding site
inner membrane
HAMP domain
coiled-coiled
domain
trimerization tip
cytoplasm
B
phase
GFP
N379R
localization profile
C
phase
GFP
G24G D249G L250G
localization profile
D
Tar-mGFP
N379R
G248G D249G
L250G
GlpT
age
local brigthness
100
90
80
70
60
50
40
30
20
10
0 50 100
0 50 100
0 50 100
0 50 100

Supporting Information

Membrane curvature and the Tol-Pal complex determine polar localization of the chemoreceptor Tar in *E. coli*

Terrens N. V. Saaki, Henrik Strahl, Leendert W. Hamoen

Content:

Supporting Table S1: *E. coli* strains used in this study. kan: kanamycin, mGFP: monomeric green fluorescent protein.

strain	relevant genotype	reference
BW25113	F-, *Δ(araD-araB)567, ΔlacZ4787(::rrnB-3), λ-, rph-1, Δ(rhaD-rhaB)568, hsdR514*	(1)
TSS688	*Δtsr-7028 Δ(tar-tap)5201 Δtrg-100 Δaer-1*	(2)
JW0731-1	BW25113 *Δpal-790::kan*	(1)
JW0729-3	BW25113 *ΔtolA788::kan*	(1)
JW1877-1	BW25113 *ΔcheA741::kan*	(1)
JW1875-5	BW25113 Δtar-739::kan	(1)
TSE24	JW1875-5 / pTNV148	this work
TSE25	JW1875-5 / pTNV149	this work
TSE29	BW25113 / pTNV149	this work
TSE31	JW0731-1 / pTNV149	this work
TSE32	JW0729-3 / pTNV149	this work
TSE38	JW1877-1 /pTNV149	this work
TSE41	BW25113 / pTNV154	this work
TSE42	BW25113 / pTNV153	this work
TSE48	BW25113 / pTNV155	this work
TSE67	BW25113 / pTNV162	this work
TSE68	JW0731-1 / pTNV153	this work
TSE69	JW0731-1 / pTNV154	this work
TSE71	JW0731-1 / pTNV162	this work
TSE79	TSS688 / pTNV149	this work
TSE80	TSS688 / pTNV153	this work
TSE81	TSS688 / pTNV154	this work

Supporting Table S2: Plasmids used in this study. *gfp*: green fluorescent protein, *mgfp*: monomeric GFP, *camR*: chloramphenicol acetyltransferase, *ampR*: β-lactamase TEM-1.

Name	Relevant feature	reference
pBAD24-tar-GFP	pBAD-*tar-gfp-ampR*	(3)
pBAD24-tar-mGFP	pBAD-*tar-mgfp-ampR*	this work
p29SEN	Rep101 pSC101 ori *ampR*	(4)
pSAV57	pTrcDown, p15Aori camR	(5)
pTNV100	*amyE3'*-spec-PxylR-*mgfp*-mcs-*amyE5'* ampR	this work
pTNV107	pBAD-*tar-mgfp-ampR* pSC101 ori araC	this work
pTNV148	P*tar-tar-mgfp-ampR*-pSC101 ori	this work
pTNV149	Ptrc-*tar-mgfp-ampR*-pSC101 ori	this work
pTNV153	Ptrc-*tar*(G248G-D249G-L250G)-*mgfp-ampR* pSC101 ori	this work
pTNV154	Ptrc-*tar*(N379R)-*mgfp-ampR* pSC101 ori	this work
pTNV155	Ptrc-*mgfp-ftsN- ampR* pSC101	this work
pTNV162	Ptrc-*mgfp-glpT-ampR*-pSC101	this work

Supporting Table S3: Primers used in this study.

name	sequence	description
TerS327	CAGGAAGCGGCTCAGGATCCTGAGTAAACTTGGTCTGACAGT	Forward primer to linearize pBAD24-tar-mGFP
TerS328	CACCGTCATCACCGAAACGCGCGA	Reverse primer to linearize pBAD24-tar-mGFP
TerS362	GGATCCTGAGCCGCTTCCTGA	Reverse primer to amplify *mgfp* from pTNV100
TerS412	CGCATGGGGAGACCCCACACTACCA	Reverse sequencing primer for pBAD vectors
TerS418	CATGGTGAATTCCTCCTGCTAGCCCA	Reverse primer to amplify pBAD24 including its RBS and start codon
TerS425	GCGTTTCGGTGATGACGGTGCGGCGGCACCTCGCTAACGGA	Forward primer to amplify origin of replication of p29SEN (pSC101 Ori)
TerS426	GGATCCTGAGCCGCTTCCTGCTTGCGCGCACCGCCCGAACACCA	Reverse primer to amplify origin of replication of p29SEN (pSC101 Ori)
TerS457	GCCGCGGTTGAAGCCGCGCGTGCGGGT	Forward primer to amplify tar in pTNV149
TerS506	GTGTGAAATTGTTATCCGCTCACA	Reverse primer to amplify Ptrcdown promoter with lacI from pSAV057
TerS507	GAGCGGATAACAATTTCACACACCCGTTTTTTTGGGCTAGCAGGAGGA	Forward primer to insert Ptrc-down promoter into pTNV107
TerS508	CGGCTTGACGGAGTAGCATAGGGT	Forward primer to insert *tar* native promoter into pTNV107
TerS509	TATGCTACTCCGTCAAGCCGGGCGCTGTTAGATAGCGCGGCGTCAGAAGTGGCGTAA	Reverse primer to insert *tar* native promoter into pTNV107
TerS510	GCCGCCTGGGCGCTGCGACTGGCA	Reverse primer to amplify inside *tar*
TerS515	CGCAGTGAAATGGGCGGAGGA[1]GCGCAGAGCGT	Forward primer to design Tar(G248G D249G L250G) in pTNV149
TerS516	CTGCGCTCCTCC[1]GCCCATTTCACTGCGCCCGTCA	Reverse primer to design Tar(G248G D249G L250G) in pTNV149
TerS517	CGCGCGGCTTCAACCGCGGCTCT[1]CAGCGCGAGGATATTAGTCT	Mutagenesis primer to introduce N379R in Tar in pTNV149
TerS520	CCGGGCAGGCCATGTCTGCCAGCGGCCGCGACTCTAGAATTCG	Forward primer to linearize pTNV149
TerS521	CTAGCAGGAGGAATTCACCATGAGCAAAGGAGAAGAACTTTTCACT	Forward primer to amplify *mgfp* from pTNV100
TerS523	GGCAGACATGGCCTGCCCGGGGGGGGGATTTTGAGGGTTTCA	Reverse primer to amplify ftsN to design Pspac-msfGFP-4GS-FtsN
TerS541	CAGGAAGCGGCTCAGGATCCGCACAACGAGATTATGTACGCCGCA	Forward primer to create Pspac-msfGFP-4GS-FtsN
TerS544	GGCAGACATGGCCTGCCCGGGCCATTAGCCTCCGTTGCGTTCTTGCA	Reverse primer to amplify *glpT*
TerS545	CAGGAAGCGGCTCAGGATCCATGTTGAGTATTTTTAAACCAGCGCCA	Forward primer to amplify *glpT*
GFP(A206K)-for	CCTGTCGACACAATCTAAACTTTCGAAAGATCCC	Forward primer to introduce A206K in GFP in pBAD24-tar-GFP
GFP(A206K)-rev	GGGATCTTTCGAAAGTTTAGATTGTGTCGACAGG	Reverse primer to introduce A206K in GFP in pBAD24-tar-GFP

1: In red codons used to introduce mutations in amino acid sequences.

Fig. S1

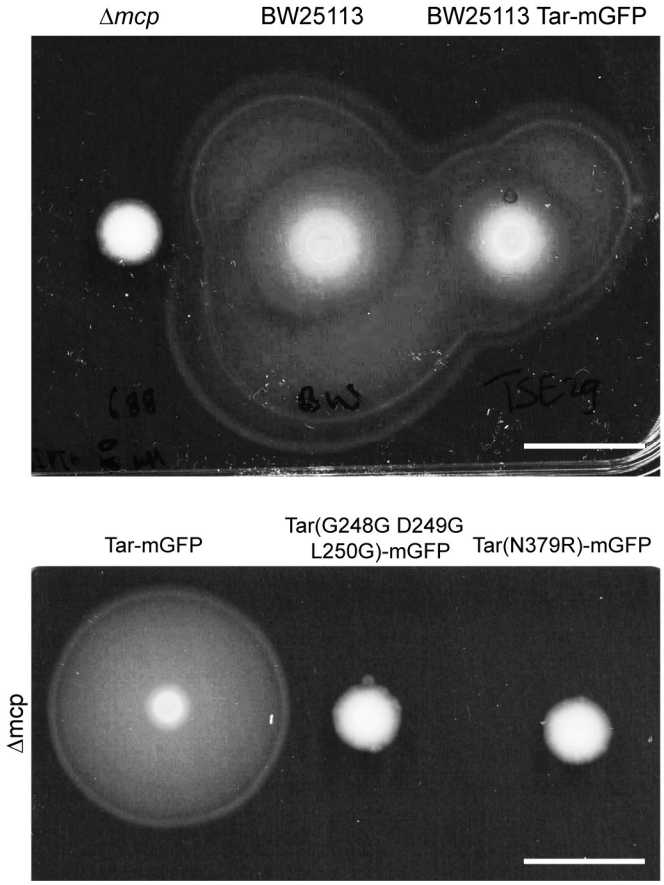

Fig. S1. Swarming motility assay

Swarming motility assay to test functionality of Tar-mGFP fusions. Representative image of colonies of *E. coli* Δmcp, *E. coli* BW25113, *E. coli* BW25113 + Tar-mGFP, *E. coli* Δmcp + Tar-mGFP, *E. coli* Δmcp + Tar(G488G D249G L250G)-mGFP and *E. coli* Δmcp Tar(N379R)-mGFP after 18 hours of growth at 30 °C on swarming motility agar. Fusion proteins were induced with 15 μM IPTG. Scale bars are 2 cm. Strain used are TSS668, BW25113, TSE29, TSE79, TSE80, and TSE81.

Fig. S2

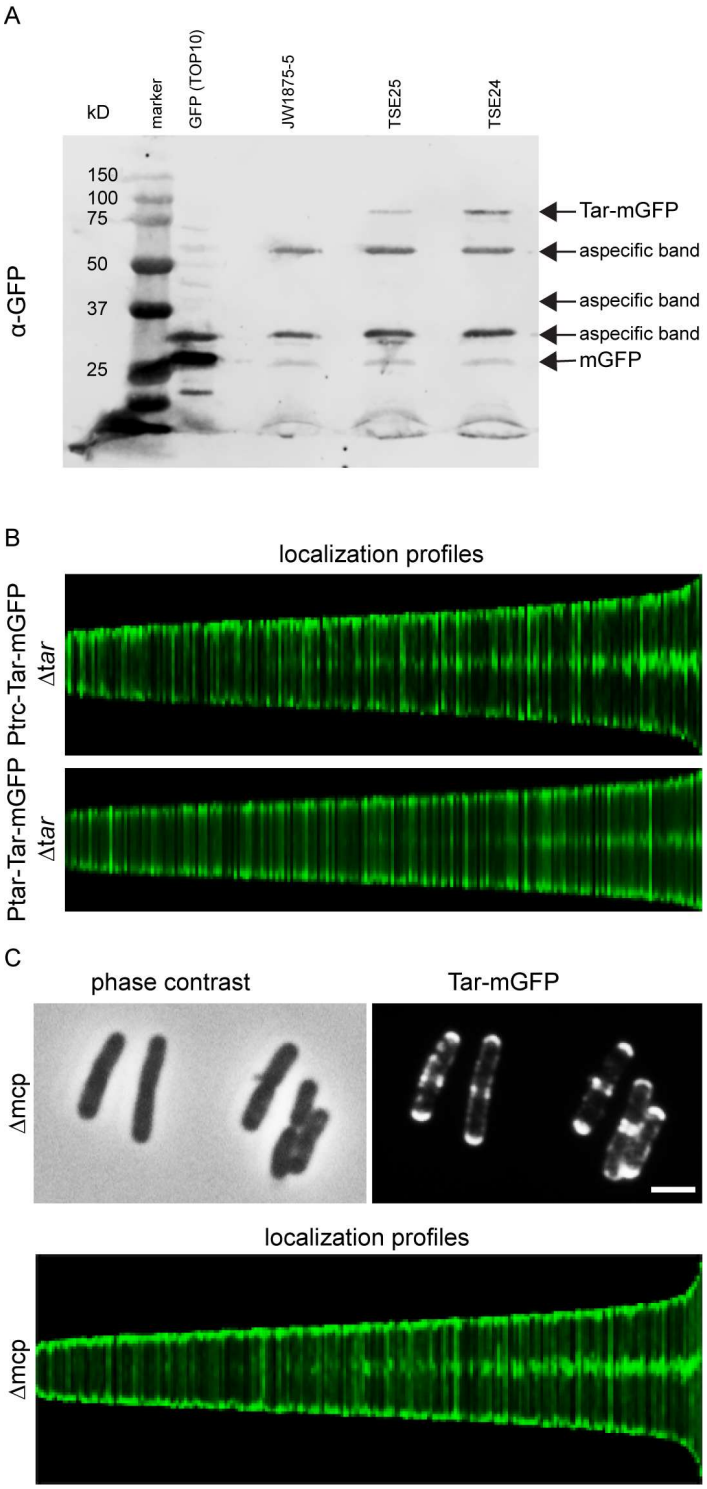

Fig. S2. Tar-mGFP expressed from native promoter and IPTG-inducible promoter.

(A) Westernblot using anti-GFP serum of cell extracts from cells constitutively expressing GFP (*E. coli* TOP 10 / pTNV100), Δ*tar* cells (JW1875-5), and cells expressing Tar-mGFP (TSE25 and TSE24). Tar-mGFP was expressed from the native promotor of *tar* (strain TSE25) or from

the IPTG-inducible (15 μM IPTG) *Ptrc* promoter (strain TSE24). The expected size for the fusion proteins is 87 kDa. Expression from the pBAD promoter is approximately 2x that of the native promoter. (B) Comparison of Tar-mGFP localization when expressed from the Ptrc promoter (upper panel) or native promoter (lower panel). 4630 and 4111 cells were used to contruct the localization profiles, respectively. (C) Phase contrast and fluorescence microscopy images and localization profile of Tar-mGFP expressed in a Δ*mcp* mutant lacking all chemoreceptors (strain TSE79). 2089 cells were used to construct the localization profile. Scale bar is 2 μm.

Fig.S3

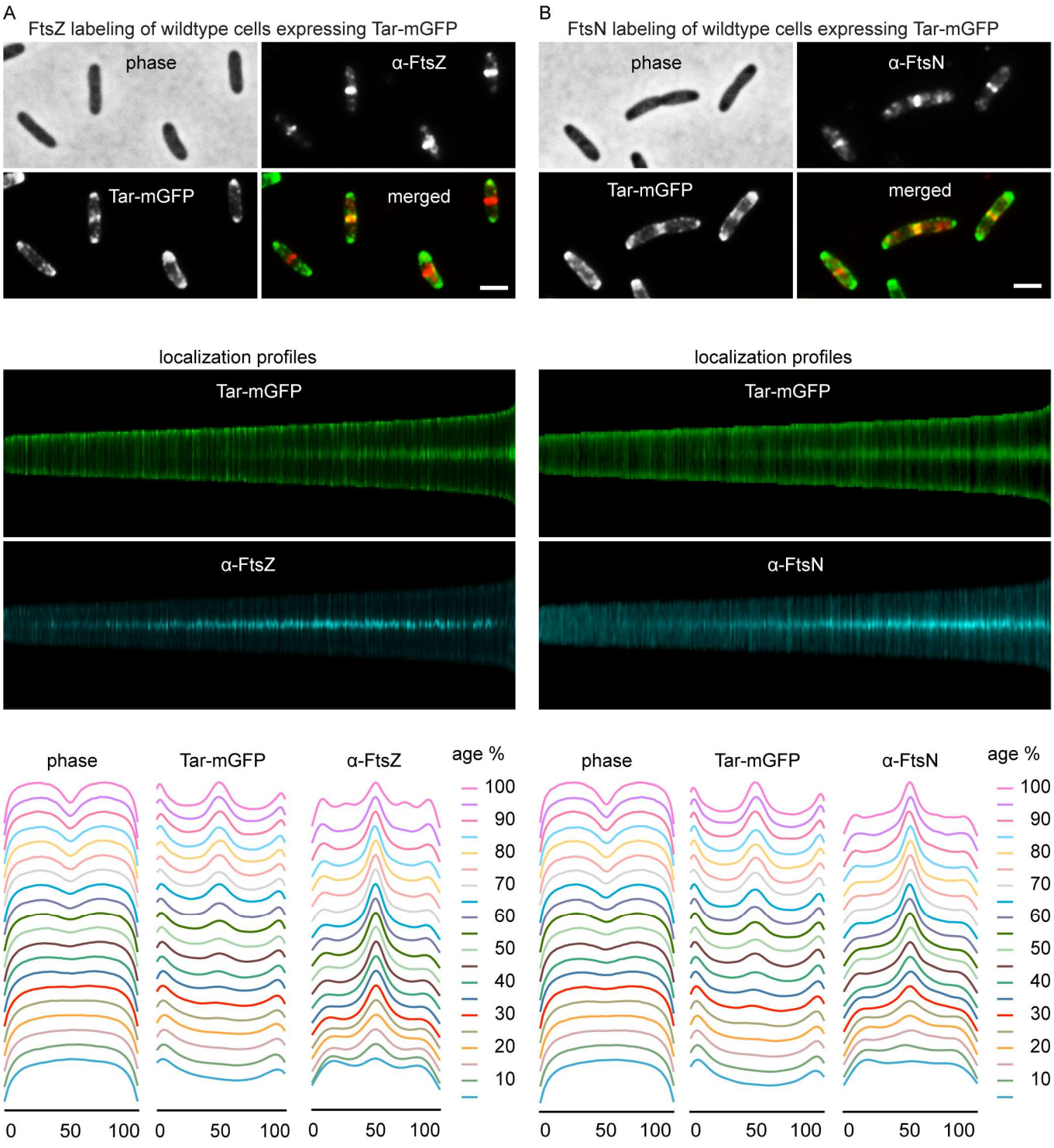

Fig. S3. Timing of Tar-mGFP midcell localization compared to FtsZ and FtsN. Tar-mGFP expressing cells were fixed and immune-labelled using FtsZ (A) and FtsN (B) antiserum. Top panel: fluorescence light microscopy images, middle panel: fluorescence localization profiles,

lower panel: graphical presentation of constriction (phase) and fluorescence signals during the cell cycle calculated from the localization profiles. Cell age refers to age classes divided in 5% (cell cycle) bins. 4816 and 3639 cells were used for FtsZ and FtsN labeling, respectively. Scale bars are 2 μm and the strain used is TSE29.

Fig. S4

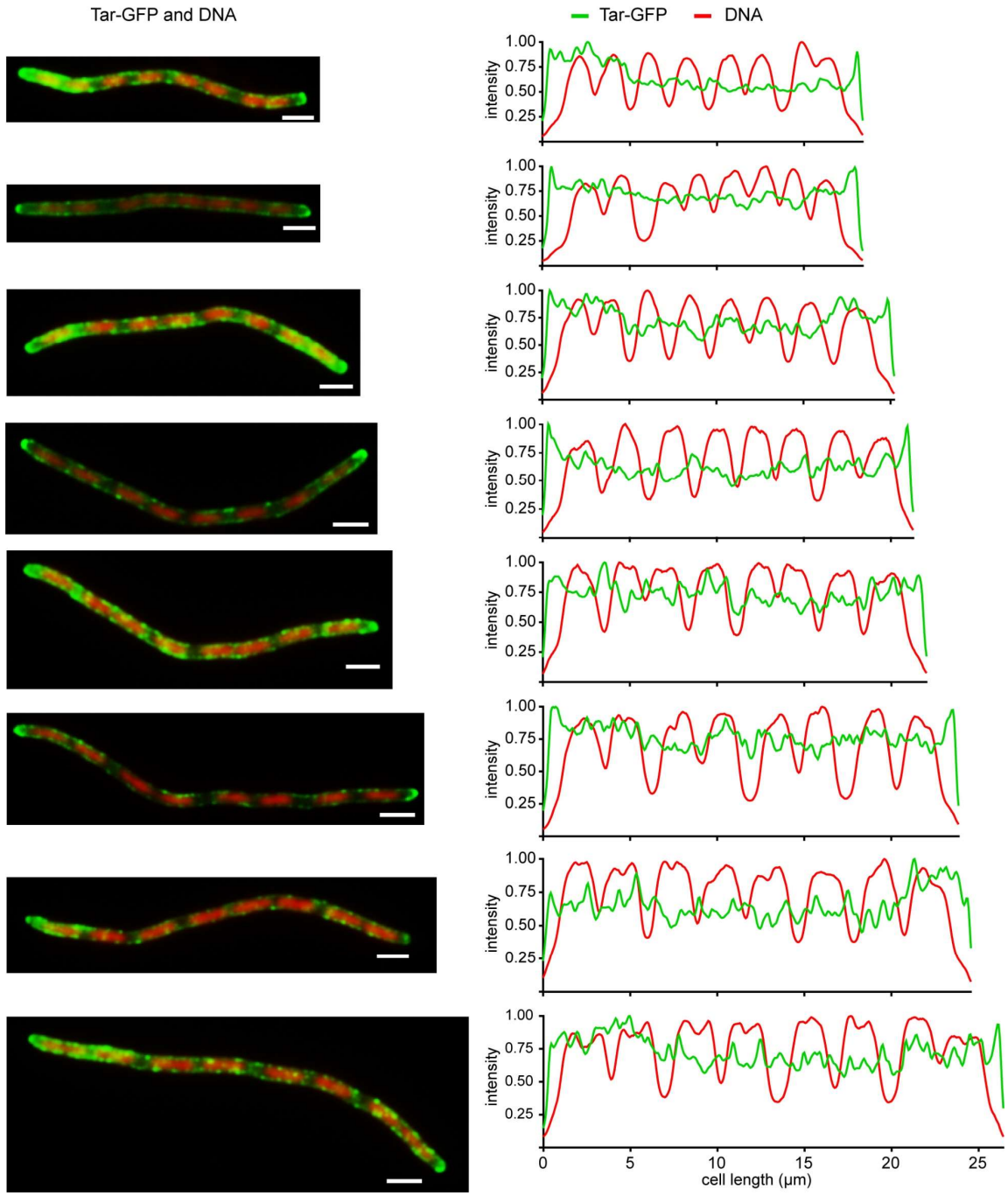

Fig. S4. Tar-GFP localization is unrelated to nucleoid position

Fluorescence microscopy images of cephalexin treated (4 h) cells expressing Tar-mGFP and stained with DAPI. Line scans of the GFP and DAPI signals are shown in the right panels. These images are more examples of cells shown in Fig. 2B in the main text. Scale bars are 2 μm. Strain used is TSE29.

Fig.S5

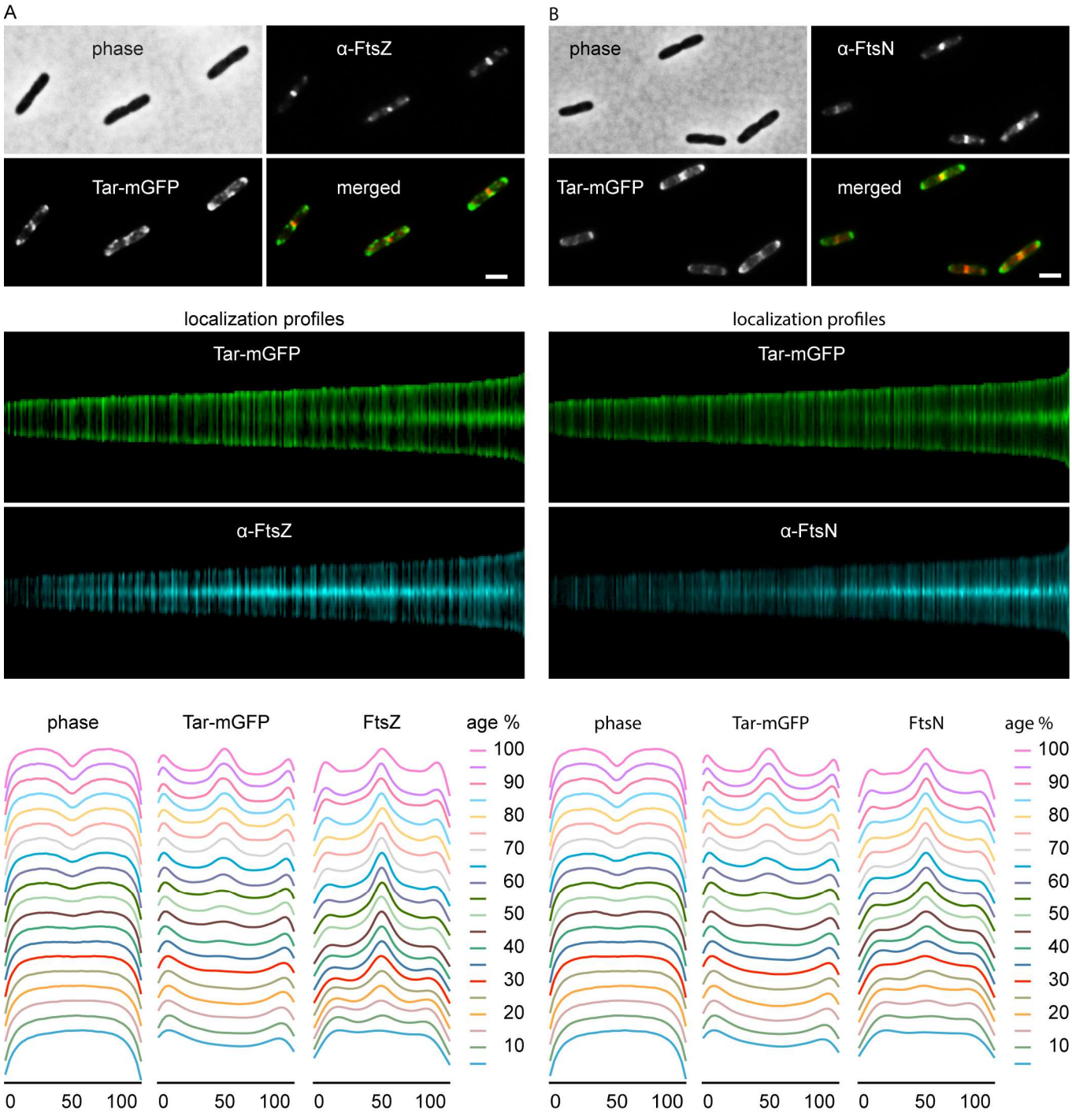

Fig. S5. Timing of Tar-mGFP midcell localization in Δ*cheA* compared to FtsZ and FtsN. Tar-mGFP expressing Δ*cheA* cells were fixed and immune-labelled using FtsZ (A) and FtsN (B) antiserum. Top panel: fluorescence light microscopy images, middle panel: fluorescence localization profiles, lower panel: graphical presentation of constriction (phase) and

fluorescence signals during the cell cycle calculated from the localization profiles. Cell age refers to age classes divided in 5% (cell cycle) bins. 2504 and 3187 cells were used for FtsZ and FtsN labeling, respectively. Scale bars are 2 μm and the strain used is TSE38.

Fig. S6

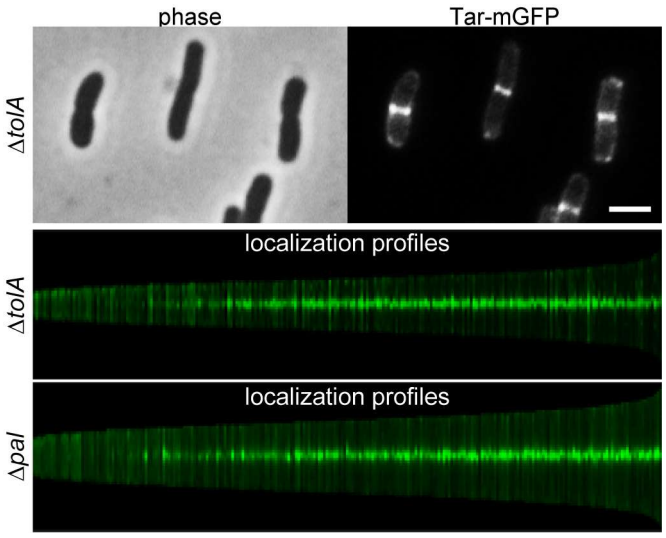

Fig S6. Tar-mGFP localization in Δ*tolA* and Δ*pal* cells

Fluorescence microscopy image and localization profiles of Tar-mGFP expressed in a Δ*tolA* and Δ*pal* background. 4506 and 9044 cells were used to construct the localization profile for Δ*tolA* and Δ*pal*, respectively. The localization profile for Δ*pal* is the same as in Fig. 3B. Scale bar is 2 μm. The strains used are TSE31 and TSE32.

Fig. S7

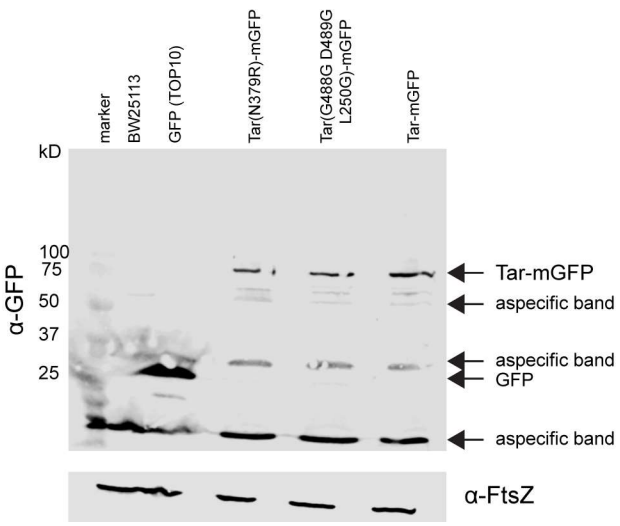

Fig. S7. Stability of Tar-mGFP mutants

Western blot analysis of Tar-mGFP mutants expressed in *E. coli*. The expected size for the fusion proteins is 87 kDa. Strains used are BW25113 (wild type), *E. coli* TOP10/pTNV100 (GFP) TSE29 (Tar-mGFP), TSE41 (Tar(G248G D249G L250G)-mGFP), and TSE42 (Tar(N379R)-mGFP).

Fig. S8

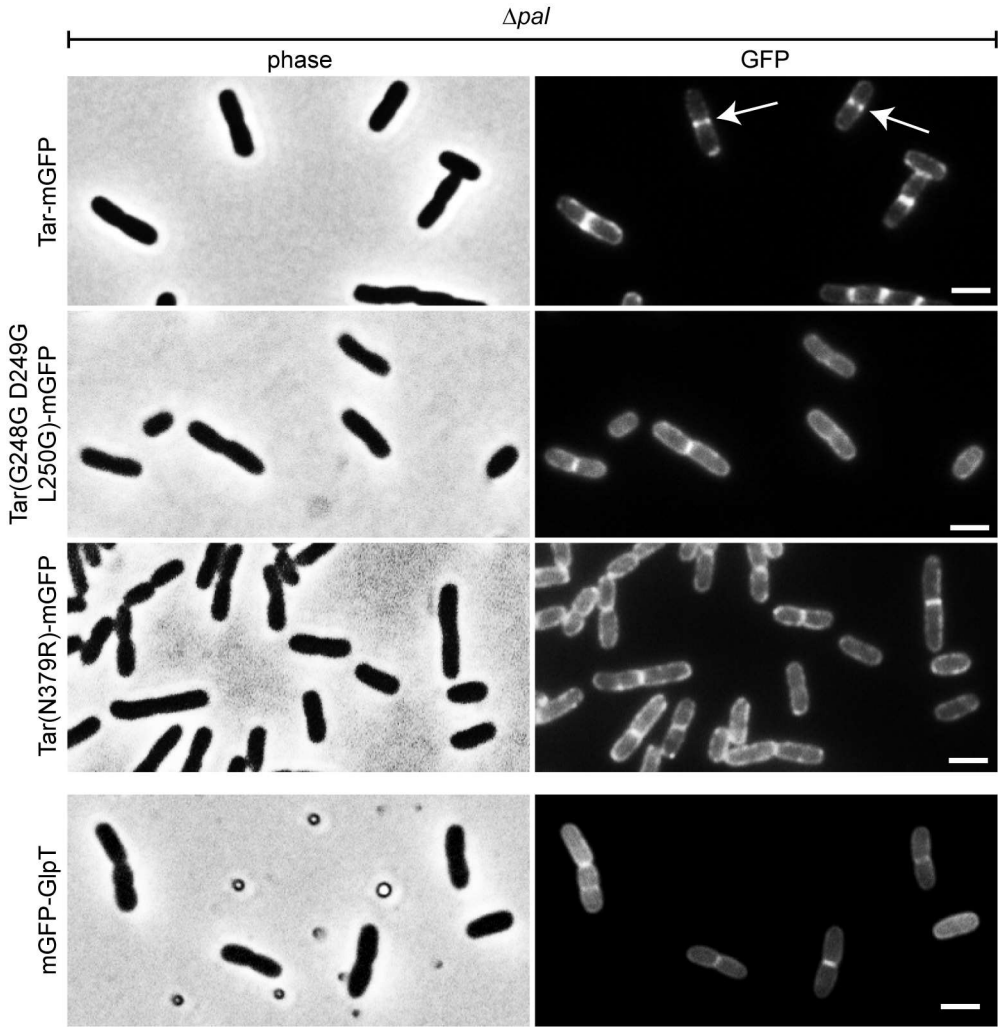

Fig. S8 Localization of Tar-mGFP mutants in Δ*pal* cells

Phase contrast and fluorescence images of Δ*pal* cells expressing Tar-mGFP, Tar-(G248G D249G L250G)-mGFP, Tar-(N379R)-mGFP and mGFP-GlpT. Wild type Tar-mGFP accumulates as two dots (white arrows) in ~47% of cells, while this accumulation was neither observed for the Tar-mGFP mutants proteins nor for the inner membrane marker mGFP-GlpT. Strain used are TSE31, TSE68, TSE69, and TSE71. The scale bars are 2 μm.

References

1. **Baba T**, **Ara T**, **Hasegawa M**, **Takai Y**, **Okumura Y**, **Baba M**, **Datsenko KA**, **Tomita M**, **Wanner BL**, **Mori H**. 2006. Construction of *Escherichia coli* K-12 in-frame, single-gene knockout mutants: the Keio collection. Molecular Systems Biology **2**:2006.0008.

2. **Ames P**, **Studdert CA**, **Reiser RH**, **Parkinson JS**. 2002. Collaborative signaling by mixed chemoreceptor teams in *Escherichia coli*. Proc Natl Acad Sci USA **99**:7060–7065.

3. **Shiomi D**, **Yoshimoto M**, **Homma M**, **Kawagishi I**. 2006. Helical distribution of the bacterial chemoreceptor via colocalization with the Sec protein translocation machinery. Mol Microbiol, 2nd ed. **60**:894–906.

4. **Genevaux P**, **Keppel F**, **Schwager F**, **Langendijk-Genevaux PS**, **Hartl FU**, **Georgopoulos C**. 2004. In vivo analysis of the overlapping functions of DnaK and trigger factor. EMBO Rep **5**:195–200.

5. **Alexeeva S**, **Gadella TWJ**, **Verheul J**, **Verhoeven GS**, **Blaauwen den T**. 2010. Direct interactions of early and late assembling division proteins in *Escherichia coli* cells resolved by FRET. Mol Microbiol **77**:384–398.